Applied Catalysis B: Environmental 123–124 (2012) 84–88

Contents lists available at SciVerse ScienceDirect

Applied Catalysis B: Environmental

journal homepage: www.elsevier.com/locate/apcatb

Ag-doped Mn–Cd sulfide as a visible-light-driven photocatalyst for H_2 evolution

Keita Ikeue*, Yumeki Shinmura, Masato Machida

Department of Applied Chemistry and Biochemistry, Graduate School of Science and Technology, Kumamoto University, 2-39-1 Kurokami, Kumamoto 860-8555, Japan

ARTICLE INFO

Article history:
Received 28 January 2012
Received in revised form 13 April 2012
Accepted 14 April 2012
Available online 21 April 2012

Keywords:
H_2 production
Sulfide
Photocatalyst
Visible light response
Ag
Hydrothermal synthesis

ABSTRACT

We have investigated the role of Ag in the $Ag_yMn_{1-x-y}Cd_xS$ during photocatalytic H_2 evolution under visible light irradiation ($\lambda > 420$ nm). The rate of H_2 evolution increased with the amount of Ag doping, and reached a maximum at $y = 0.003$ ($x = 0.40$). $Ag_yMn_{1-x-y}Cd_xS$ consisted of a highly crystalline solid solution phase over the range $0.48 \le x \le 0.63$ and $0 \le y \le 0.02$, suggesting that the effect of Ag on the photocatalytic activity is not associated with crystallinity. UV–vis absorption spectra of $Ag_yMn_{1-x-y}Cd_xS$ showed a band gap absorption at 500 nm and a flat absorption above 500 nm. The latter absorption was caused by the presence of Ag_2S, which does not significantly contribute to the photocatalytic activity. X-ray photoelectron spectroscopy detected metallic Ag on the surface of $Ag_{0.003}Mn_{0.40}Cd_{0.60}S$, which could act as a co-catalyst in photocatalytic hydrogen evolution.

© 2012 Elsevier B.V. All rights reserved.

1. Introduction

Photocatalytic water splitting using sunlight as an inexhaustible energy source to produce H_2 has attracted intense interest [1]. To harness the solar energy, visible-light-driven photocatalysts need to be developed. Many photocatalysts have been developed over the past few decades, including oxide-, sulfide-, and oxynitride-based materials [2–11]. Sulfide- and oxynitride-based materials are the most promising photocatalysts because of their visible light response. Pt-loaded CdS shows high photocatalytic activity for H_2 evolution from a solution containing sacrificial agents [12–16]; other metal sulfides show low photocatalytic activity for water splitting, although their activities are improved by metal doping [17,18] and the formation of a solid solution of two different metal sulfides. Kudo et al. reported that a series of solid solutions of ZnS and a variety of sulfide-based semiconductors produced highly efficient composite sulfide photocatalysts [19–21]. However, their apparent quantum yields for H_2 evolution in the visible light region were less than 20%.

We have previously reported that hydrothermally synthesized $Mn_{1-x}Cd_xS$ with a high Mn content ($x = 0.17$) showed high photocatalytic activity for H_2 evolution under visible light irradiation ($\lambda > 420$ nm) [22,23]. $Mn_{1-x}Cd_xS$ consists of an active low crystalline solid solution phase and an inactive wurtzite type γ-MnS phase. Doping $Mn_{1-x}Cd_xS$ with Ni, Cu, and Ag enhanced the photocatalytic activity in the order $Ni_{0.01}Mn_{0.51}Cd_{0.48}S > Ag_{0.01}Mn_{0.36}Cd_{0.63}S > Cu_{0.01}Mn_{0.57}Cd_{0.42}S$, where ($y = 0.01$). The quantum yield at $\lambda = 420$ nm for H_2 evolution of the Ni-doped sample reached 25%. Structural studies of the Ni-doped samples showed that the crystallinity of solid solution phase was increased by metal doping, and this enhanced the photocatalytic activity. However, the effect of metal doping on the photocatalytic activity of other metal-doped Mn–Cd–S catalysts is not well explored. Accordingly, we focused on the secondary active photocatalyst, the Ag-doped sample, in order to investigate the effect of metal doping on the photocatalytic activity of Mn–Cd–S.

We examined the crystal structure, optical absorption properties, and oxidation state of Ag for the Ag-doped sample by X-ray diffraction (XRD), UV–vis absorption spectroscopy, and X-ray photoelectron spectroscopy (XPS). On the basis of these spectroscopic findings, we have elucidated the role of Ag doping in improving the photocatalytic activity of the catalyst.

2. Experimental

2.1. Catalyst preparation and characterization

Composite sulfides, $Ag_yMn_{1-x-y}Cd_xS$ ($0.48 \le x \le 0.6$, $0 \le y \le 0.02$), were synthesized by a hydrothermal method. A mixture of $Cd(CH_3COO)_2{\cdot}2H_2O$ ($10x$ mmol), $Mn(CH_3COO)_2{\cdot}4H_2O$ ($10 - 10(x + y)$ mmol), $Ag(CH_3COO)$ ($10y$ mmol), and thioacetamide (10–20 mmol), and distilled water (30 mL) was placed in a stainless steel reaction vessel (150 mL) and heated at 180 °C for 24 h without stirring. The reagents (99.9%) were purchased from Wako Pure

* Corresponding author. Tel.: +81 96 342 3653; fax: +81 96 342 3653.
E-mail address: ikeue@kumamoto-u.ac.jp (K. Ikeue).

0926-3373/$ – see front matter © 2012 Elsevier B.V. All rights reserved.
http://dx.doi.org/10.1016/j.apcatb.2012.04.019

Table 1
Photocatalytic activity of 1 wt% Pt-loaded Mn–Cd-based sulfides under visible light irradiation (λ > 420 nm).

Photocatalyst	S_{BET}[a] ($m^2\ g^{-1}$)	H_2 evolution rate[b] ($\mu mol\ h^{-1}$)
$Mn_{0.52}Cd_{0.48}S$	3.4	387
$Ag_{0.001}Mn_{0.40}Cd_{0.60}S$	2.4	805
$Ag_{0.003}Mn_{0.40}Cd_{0.60}S$	1.8	880
$Ag_{0.005}Mn_{0.37}Cd_{0.63}S$	1.8	638
$Ag_{0.01}Mn_{0.36}Cd_{0.63}S$	2.4	654
$Ag_{0.02}Mn_{0.34}Cd_{0.64}S$	2.4	643

[a] BET surface area.
[b] Measured in an external irradiation quartz cell under irradiation from a 500 W Xe lamp, with 0.1 M Na_2S and 0.5 M Na_2SO_3 aq. (200 mL), and catalyst (0.2 g).

Chemicals and used without further treatment. Precipitates were washed with distilled water and ethanol, and then collected by centrifugation. The centrifugation of the products gave rise to two different precipitate layers (see Supplementary data, Fig. S-1). The upper layer was a greenish yellow single-phase Ag-Mn–Cd–S solid solution, whereas the lower layer was a dark-green single-phase α-MnS. After drying at room temperature under vacuum, the greenish yellow Mn–Cd–S solid solution powder was separated from the dark-green powder. The Mn/Cd ratio of the product obtained after separation differed from that of precursor mixture because of the removal of the α-MnS phase. Therefore, it was difficult to control the composition of the sample after separation.

The crystal structure of the desiccated solid was identified by powder X-ray diffraction (XRD; Rigaku, Multiflex) with monochromated Cu Kα radiation (40 kV, 20 mA). Energy-dispersive X-ray fluorescence (XRF; Horiba, MESA-500 W) analysis was used to determine the chemical compositions. Diffuse reflectance absorption spectra were recorded on a UV–vis spectrometer (JASCO V-550) in order to determine the optical band gap energy. X-ray photoelectron spectroscopy (XPS) spectra were recorded on a spectrometer (VG Sigmaprobe) using Al Kα radiation (15 kV, 6.7 mA). The binding-energy calculation was verified using the C 1s peak position as an internal reference. The charging effect was ruled out in the measurement because the C 1s binding energy was identical for all the samples. The normal operating pressure in the analysis chamber was maintained at less than 10^{-6} Pa during the measurement.

2.2. Photocatalytic reaction

The photocatalytic reaction was carried out in an external-irradiation quartz cell connected to a closed gas-circulating system. The photocatalyst (0.2 g) was suspended in an aqueous solution of 0.1 M Na_2S and 0.5 M Na_2SO_3 (200 mL) in the cell. The rate of H_2 evolution was determined by gas chromatography (Shimadzu GC-8A, TCD, Ar carrier, MS-5A) under irradiation from a 500 W Xe lamp with a cut-off filter (λ > 420 nm). The apparent quantum yield was measured by using a monochromator and a Si photodiode. The photocatalytic reaction was also carried out after Pt photodeposition (1 wt%) on the composite sulfides from an aqueous solution of H_2PtCl_6 (Wako Pure Chemicals).

3. Results and discussion

Table 1 summarizes the rate of H_2 evolution under visible light irradiation (λ > 420 nm) for $Ag_yMn_{1-x-y}Cd_xS$ with different Ag content. The rate of H_2 evolution increased as the amount of Ag doping increased, and it reached a maximum of 880 $\mu mol\ H_2\ h^{-1}$ at $y = 0.003$, which is more than two-fold that of undoped $Mn_{0.52}Cd_{0.48}S$. However, further increases in the Ag content decreased the rate of H_2 evolution. The 4 h photocatalytic test using the Ag-doped sample ($y = 0.003$) could be repeated three times without noticeable deactivation and the total amount of H_2 evolution per mole of photocatalyst reached more than 5.5 mol/mol (see Supplementary data, Fig. S-2). These results demonstrate that doping Mn–Cd sulfide with small amounts of Ag can significantly improve its photocatalytic activity.

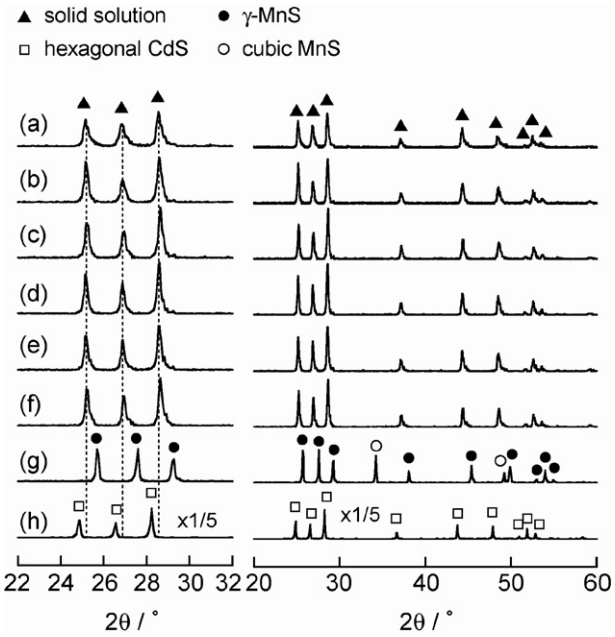

Fig. 1. XRD patterns of (a) $Mn_{0.52}Cd_{0.48}S$, (b) $Ag_{0.001}Mn_{0.40}Cd_{0.60}S$, (c) $Ag_{0.003}Mn_{0.40}Cd_{0.60}S$, (d) $Ag_{0.005}Mn_{0.37}Cd_{0.63}S$, (e) $Ag_{0.01}Mn_{0.36}Cd_{0.63}S$, (f) $Ag_{0.02}Mn_{0.34}Cd_{0.64}S$, (g) γ-MnS, and (h) hexagonal CdS. The left figure shows the lower angle region ($22^\circ < \theta < 32^\circ$) of the right figure.

The photocatalytic activity is influenced by the surface area, particle size, and crystallinity. These factors are related to the charge transfer and recombination processes of photogenerated electrons and holes. In addition, metal doping may lead to the formation of an impurity level, which acts as an electron donor and acceptor or as a recombination center. The effect of surface area on photocatalytic activity can be negligible because there is not large difference in the BET surface areas of our Mn–Cd sulfides (1.8–3.4 $m^2\ g^{-1}$). Therefore, the effect of Ag doping on photocatalytic activity has several possible explanations: (1) the crystallinity of the active phase is influenced by metal doping; (2) the impurity level formed by metal doping affects the recombination of photogenerated electrons and holes; (3) the doped metals act as a co-catalyst, enhancing the photocatalytic activity.

In order to test these explanations, we investigated the crystallinity and optical absorption of the samples by XRD and UV–vis absorption spectroscopy, respectively. Fig. 1 shows the XRD patterns of hydrothermally synthesized $Ag_yMn_{1-x-y}Cd_xS$, $Mn_{0.52}Cd_{0.48}S$, MnS ($x = 0$, $y = 0$), and CdS ($x = 1$, $y = 0$). The diffraction patterns showed that the MnS contained a mixture of cubic (α, rock-salt type) and hexagonal (γ, wurtzite type) phases, whereas CdS consisted of a single of hexagonal (wurtzite type) phase. The three intense peaks of the undoped sample ($Mn_{0.52}Cd_{0.48}S$) at $2\theta < 30^\circ$ were shifted toward the lower values of 2θ compared with the hexagonal MnS phase, indicating that the peaks observed in the undoped sample can be assigned to the solid solution phase. The diffraction peaks observed in the $Ag_yMn_{1-x-y}Cd_xS$ series can thus be assigned to the solid solution phase by comparison with the undoped sample. The peak width and intensity were similar over the range $0.48 \le x \le 0.63$, and $0 \le y \le 0.02$. These results demonstrate that the effect of Ag on the photocatalytic activity is not associated with the crystallinity.

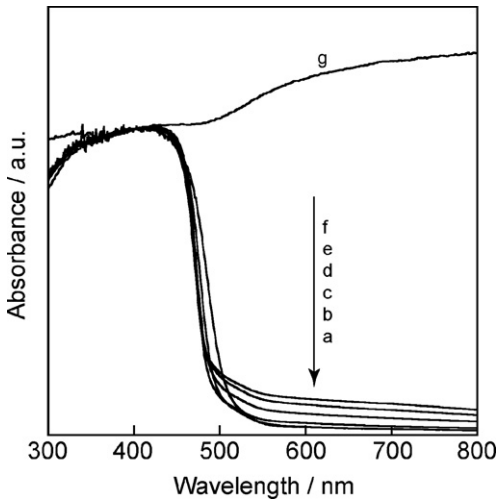

Fig. 2. UV–vis absorption spectra of (a) $Mn_{0.52}Cd_{0.48}S$, (b) $Ag_{0.001}Mn_{0.40}Cd_{0.60}S$, (c) $Ag_{0.003}Mn_{0.40}Cd_{0.60}S$, (d) $Ag_{0.005}Mn_{0.37}Cd_{0.63}S$, (e) $Ag_{0.01}Mn_{0.36}Cd_{0.63}S$, and (f) $Ag_{0.02}Mn_{0.34}Cd_{0.64}S$, (g) Ag_2S.

Fig. 2 shows the UV–vis absorption spectra of $Ag_yMn_{1-x-y}Cd_xS$. All the Ag-doped samples showed an absorption edge at around 500 nm, which suggests that the band gap energy was 2.6 eV. This is slightly higher than that of the undoped sample (2.5 eV). A flat absorption was observed at $\lambda > 500$ nm, which increased with Ag content. There are two possible explanations for this observation: (1) the excitation from the acceptor levels formed by the Ag doping, and (2) the absorption of Ag_2S, as shown in Fig. 2. If the absorption in the wavelength region of $\lambda > 500$ nm was due to excitation from the acceptor level, the onset of the action spectrum would appear at $\lambda > 500$ nm. To examine the effect of the absorption at $\lambda > 500$ nm on the photocatalytic activity, the apparent quantum yield was measured at different wavelengths for $Ag_{0.02}Mn_{0.34}Cd_{0.64}S$ and $Ag_{0.003}Mn_{0.40}Cd_{0.60}S$. $Ag_{0.02}Mn_{0.34}Cd_{0.64}S$ showed a larger absorbance at $\lambda > 500$ nm than $Ag_{0.003}Mn_{0.40}Cd_{0.60}S$. Fig. 3 shows the action spectra for the H_2 evolution for $Ag_{0.003}Mn_{0.40}Cd_{0.60}S$ and $Ag_{0.02}Mn_{0.34}Cd_{0.64}S$. The onset of action spectra was observed at $\lambda < 500$ nm for both photocatalysts. This result suggests that the absorption is not caused by excitation from the acceptor level. The effect of transition metal doping on the photocatalytic activity of TiO_2 has previously been reported [24–26]. The metal doping was accompanied by the formation of a broad absorption band which was attributed to the impurity level in the visible light region, and this accelerated the recombination of photogenerated electrons and holes. For TiO_2, the doped samples generally showed a lower photocatalytic activity than the undoped sample. Conversely, all the Ag-doped samples in our study showed a higher photocatalytic activity than the undoped sample. This indicates that the decrease in the photocatalytic activity with the increase in Ag content was not caused by the formation of an impurity level, and the absorption band at $\lambda > 500$ nm did not arise from the formation of an acceptor level and an impurity level. The increase in the absorption in the visible light region (>500 nm) was not associated with the improvement in photocatalytic activity.

To determine the oxidation state of the Ag species, Ag3d XPS spectra were obtained. Fig. 4 shows the Ag3d XPS spectra of $Ag_{0.003}Mn_{0.40}Cd_{0.60}S$ and $Ag_{0.02}Mn_{0.34}Cd_{0.64}S$. The $Ag3d_{5/2}$ XPS spectrum of $Ag_{0.003}Mn_{0.40}Cd_{0.60}S$ showed a metallic Ag peak at 368.5 eV [27–30], and a peak at 365.5 eV from Ag^+ in Ag_2O [31]. The Ag_2S peak, which should appear at 367.8 eV [27–30], was not detected in $Ag_{0.003}Mn_{0.40}Cd_{0.60}S$, whereas the $Ag3d_{5/2}$ spectrum of $Ag_{0.02}Mn_{0.34}Cd_{0.64}S$ showed the peak at 368.0 eV. This is in an intermediate peak position between metallic Ag and Ag_2S similar to that of bulk Ag_2S, which indicates that the Ag_2S concentration of $Ag_{0.02}Mn_{0.34}Cd_{0.64}S$ is >90%. Under our sulfide synthesis conditions, it is possible that hydrogen sulfide is formed during the hydrothermal treatment. The reducibility of the metal ions increases in the order $Ag^+ > Cd^{2+} > Mn^{2+}$, because the change in free energy, ΔG, for the reduction of metal ion is $-84.9\,kJ\,mol^{-1}$ for Ag^+/Ag, $77.2\,kJ\,mol^{-1}$ for Cd^{2+}/Cd, $208.4\,kJ\,mol^{-1}$ for Mn^{2+}/Mn. Ag is the most easily reduced element present, which means that the

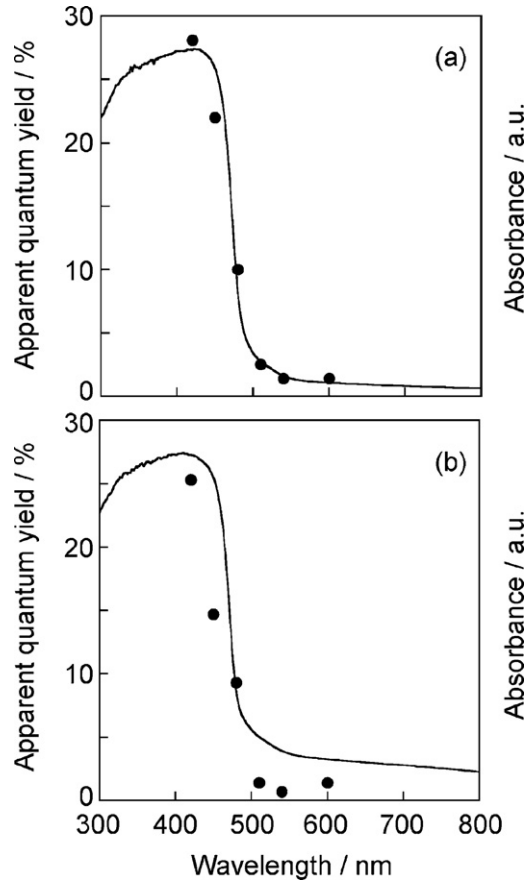

Fig. 3. Wavelength dependence of the apparent quantum yield of (a) $Ag_{0.003}Mn_{0.40}Cd_{0.60}S$ and (b) $Ag_{0.02}Mn_{0.34}Cd_{0.64}S$.

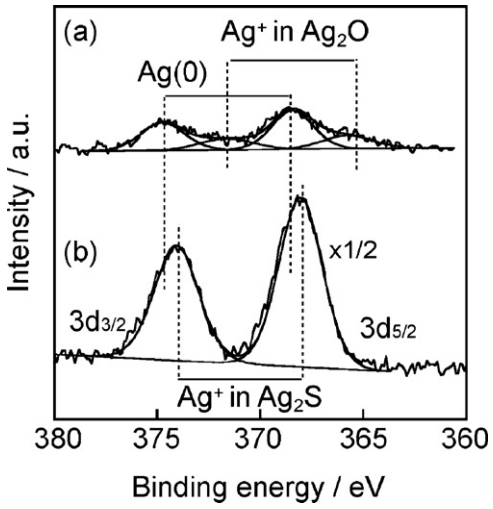

Fig. 4. Ag3d XPS spectra of (a) $Ag_{0.003}Mn_{0.40}Cd_{0.60}S$ and (b) $Ag_{0.02}Mn_{0.34}Cd_{0.64}S$.

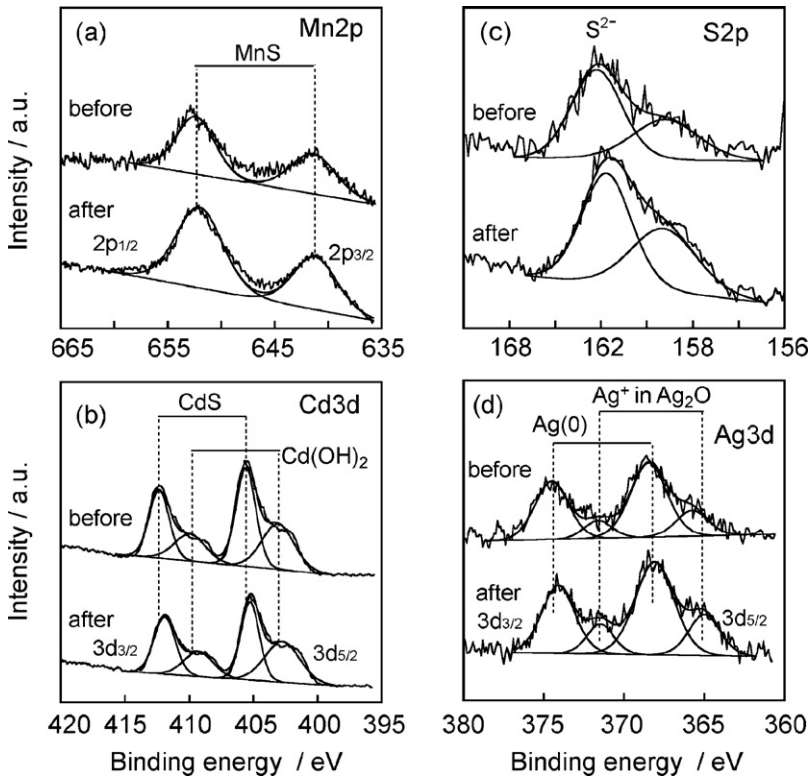

Fig. 5. XPS spectra for (a) Mn2p, (b) Cd3d, (c) S2p, and (d) Ag3d of $Ag_{0.003}Mn_{0.40}Cd_{0.60}S$ before and after the photocatalytic reaction.

Ag species in Mn–Cd–S could be partially reduced by hydrogen sulfide to form metallic Ag. The XPS and optical absorption results suggest that the absorption at $\lambda > 500$ nm in the UV spectrum of $Ag_{0.02}Mn_{0.34}Cd_{0.64}S$ can be attributed to that of Ag_2S.

XPS analysis showed that the Ag-doped sample with the highest photocatalytic activity contained metallic Ag. Metallic species loaded on photocatalysts are known to act electron-trapping sites in various photocatalytic systems [11]. The metallic Ag in the Ag-doped sample could, therefore, act as a co-catalyst in our metal-loaded photocatalysts. To verify the role of the surface Ag species, the photocatalytic test was conducted for 0.1 wt% Ag-loaded Mn–Cd–S, which was prepared by a photodeposition method (Table 2). The presence of the metallic Ag species on the Ag-loaded sample was confirmed by XPS (see Supplementary data, Fig. S-3). The photocatalytic activity of the undoped sample (entry 1) was improved by a loading of 0.1% Ag (entry 2) or 1% Pt (entry 3). However, the H_2 evolution rate for these samples was less than that of the 1% Pt/Ag doped sample (entry 4). In contrast, the rate of H_2 evolution for the 1% Pt and 0.1% Ag co-loaded Mn–Cd–S (entry 5) is similar to that for the 1% Pt/Ag-doped sample (entry 4). The electron transfer to the metallic Ag can promote the charge separation of photogenerated electrons and holes. Because of this charge separation effect, the photogenerated electrons reacted efficiently with the water molecules. However, the increase in Ag content led to a decrease in the metallic Ag species, because of the formation of Ag_2S. The deactivation of the catalyst with the increase in Ag content is caused by a decrease in the metallic Ag species, which is a promoter for charge separation. Furthermore, we checked the surface oxidation state of the sample after photocatalytic reaction by XPS (Fig. 5). No notable change in the oxidation state of each element was observed after the photocatalytic reaction. The surface atomic ratios of each element were unchanged before and after the photocatalytic reaction except for S atom (see Supplementary data, Table S-1). The increase in S atom after photocatalytic reaction can be due to adsorption of S^{2-} anion in the sacrificial agent. Consequently, the photocatalytic reaction can be repeated because the oxidation state of the surface elements is stable and the leaching of metal cation is prevented.

Table 2
Photocatalytic H_2 evolution for Ag-doped and 0.1% Ag-loaded samples.

Entry	Photocatalyst	H_2 evolution rate[a] (μmol h^{-1})
1	$Mn_{0.52}Cd_{0.48}S$	260
2	0.1%Ag/$Mn_{0.52}Cd_{0.48}S$	380
3	1%Pt/$Mn_{0.52}Cd_{0.48}S$	387
4	1%Pt/$Ag_{0.003}Mn_{0.40}Cd_{0.60}S$	880
5	1%Pt + 0.1%Ag/$Mn_{0.52}Cd_{0.48}S$	795

[a] The photocatalytic reaction was conducted as described in Table 1.

4. Conclusions

$Ag_yMn_{1-x-y}Cd_xS$ photocatalysts, which contained various amounts of Ag, achieved a 2-fold higher rate of H_2 evolution than the undoped catalyst ($Mn_{1-x}Cd_xS$). The effect of Ag doping on the photocatalytic activity was investigated in terms of the crystallinity of the active phase, the optical absorption, and the Ag surface oxidation state. The crystallinity of the active solid solution phase was negligible in improving the photocatalytic activity. The Ag_2S absorption and the band gap absorption were observed in the UV–vis absorption spectra of the $Ag_yMn_{1-x-y}Cd_xS$ samples with high Ag content. The increase in this absorption, which was caused by excess Ag doping, deactivated the photocatalyst. The metallic Ag that was detected on the surface of the Ag-doped sample acts as the co-catalyst and enhances the photocatalytic activity.

Appendix A. Supplementary data

Supplementary data associated with this article can be found, in the online version, at http://dx.doi.org/10.1016/j.apcatb.2012.04.019.

References

[1] M.G. Walter, E.L. Warren, J.R. McKone, S.W. Boettcher, Q. Mi, E.A. Santori, N.S. Lewis, Chemical Reviews 110 (2010) 6446–6473.
[2] K. Domen, J.N. Kondo, M. Hara, T. Takata, Bulletin of the Chemical Society of Japan 73 (2000) 1307–1331.
[3] A. Kudo, Catalysis Surveys from Asia 7 (2003) 31–38.
[4] J.S. Lee, Catalysis Surveys from Asia 9 (2005) 217–227.
[5] A. Kudo, The International Journal of Hydrogen Energy 31 (2006) 197–202.
[6] A. Kudo, The International Journal of Hydrogen Energy 32 (2007) 2673–2678.
[7] K. Maeda, K. Domen, Journal of Physical Chemistry C 111 (2007) 7851–7861.
[8] F.R. Osterloh, Chemistry of Materials 20 (2008) 35–54.
[9] A. Kudo, Y. Miseki, Chemical Society Reviews 38 (2009) 253–278.
[10] K. Maeda, K. Domen, The Journal of Physical Chemistry Letters 1 (2010) 2655–2661.
[11] X. Chen, S. Shen, L. Guo, S.S. Mao, Chemical Reviews 110 (2010) 6503–6570.
[12] M. Matsumura, S. Furukawa, Y. Sato, H. Tsubomura, Journal of Physical Chemistry 89 (1985) 1327–1329.
[13] J.S. Jang, U.A. Joshi, J.S. Lee, Journal of Physical Chemistry C 111 (2007) 13280–13287.
[14] D. Jing, L. Guo, Journal of Physical Chemistry B 110 (2006) 11139–11145.
[15] N. Bao, L. Shen, T. Takata, K. Domen, A. Gupta, K. Yanagisawa, C.A. Grimes, Journal of Physical Chemistry C 111 (2007) 17527–17534.
[16] L.A. Silva, S.Y. Ryu, J. Choi, W. Choi, M.H.R. Hoffmann, Journal of Physical Chemistry C 112 (2008), 12609–12073.
[17] A. Kudo, R. Niishiro, A. Iwase, H. Kato, Chemical Physics 339 (2007) 104–110.
[18] T. Arai, S. Senda, Y. Sato, H. Takahashi, K. Shinoda, B. Jeyadevan, K. Tohji, Chemistry of Materials 20 (2008) 1997–2000.
[19] I. Tsuji, H. Kato, A. Kato, Angewandte Chemie International Edition 44 (2005) 3565–3568.
[20] I. Tsuji, H. Kato, H. Kobayashi, A. Kudo, Chemistry of Materials 18 (2006) 1969–1975.
[21] I. Tsuji, Y. Shimodaira, H. Kato, H. Kobayashi, A. Kudo, Chemistry of Materials 22 (2010) 1402–1409.
[22] K. Ikeue, S. Shiiba, M. Machida, Chemistry of Materials 22 (2010) 743–745.
[23] K. Ikeue, S. Shiiba, M. Machida, ChemSusChem 4 (2011) 269–273.
[24] S. Ikeda, N. Sugiyama, B. Pal, G. Marci, L. Palmisano, H. Noguchi, K. Uosaki, B. Ohtani, Physical Chemistry Chemical Physics 3 (2001) 267–273.
[25] Z. Luo, Q.H. Gao, Journal of Photochemistry and Photobiology A 63 (1992) 367–375.
[26] N. Serpone, D. Lawless, Langmuir 10 (1994) 643–652.
[27] H.J. Zhai, H.S. Wang, Materials Research Bulletin 43 (2008) 2354–2360.
[28] J. Vinkevičius, I. Možginskienė, V. Jasulaitienė, Journal of Electroanalytical Chemistry 442 (1998) 73–83.
[29] G. Hode, S.B. Ildage, K.C. Khiar, Colloids and Surfaces A: Physicochemical and Engineering Aspects 293 (2007) 5–12.
[30] E. Tomaszewicz, M. Kurzawa, The Journal of Materials Sciences 39 (2004) 2183–2185.
[31] T.C. Kaspar, T.C. Droubay, S.A. Chambers, Thin Solid Films 519 (2010) 635–640.